Science Bulletin 66 (2021) 771–776

Contents lists available at ScienceDirect

Science Bulletin

journal homepage: www.elsevier.com/locate/scib

Article

Engineering of multiferroic $BiFeO_3$ grain boundaries with head-to-head polarization configurations

Mingqiang Li [a,b,c,1], Shuzhen Yang [d,e,i,1], Ruochen Shi [a,b], Linglong Li [i], Ruixue Zhu [a,b], Xiaomei Li [f], Yang Cheng [c,g], Xiumei Ma [a], Jingmin Zhang [a], Kaihui Liu [c,g], Pu Yu [h,i,*], Peng Gao [a,b,c,h,*]

[a] Electron Microscopy Laboratory, School of Physics, Peking University, Beijing 100871, China
[b] International Center for Quantum Materials, School of Physics, Peking University, Beijing 100871, China
[c] Academy for Advanced Interdisciplinary Studies, Peking University, Beijing 100871, China
[d] Peking University Shenzhen Graduate School, Peking University, Shenzhen 518055, China
[e] TCL China Star Optoelectronics Technology Co., Ltd., Shenzhen 518132, China
[f] Beijing National Laboratory for Condensed Matter Physics and Institute of Physics, Chinese Academy of Sciences, Beijing 100190, China
[g] State Key Laboratory for Mesoscopic Physics, School of Physics, Peking University, Beijing 100871, China
[h] Collaborative Innovation Centre of Quantum Matter, Beijing 100871, China
[i] State Key Laboratory of Low Dimensional Quantum Physics and Department of Physics, Tsinghua University, Beijing 100084, China

ARTICLE INFO

Article history:
Received 14 August 2020
Received in revised form 30 October 2020
Accepted 14 December 2020
Available online 29 December 2020

Keywords:
Head-to-head
Grain boundaries
Atomic structure
$BiFeO_3$

ABSTRACT

Confined low dimensional charges with high density such as two-dimensional electron gas (2DEG) at interfaces and charged domain walls in ferroelectrics show great potential to serve as functional elements in future nanoelectronics. However, stabilization and control of low dimensional charges is challenging, as they are usually subject to enormous depolarization fields. Here, we demonstrate a method to fabricate tunable charged interfaces with ~77°, 86° and 94° head-to-head polarization configurations in multiferroic $BiFeO_3$ thin films by grain boundary engineering. The adjacent grains are cohesively bonded and the boundary is about 1 nm in width and devoid of any amorphous region. Remarkably, the polarization remains almost unchanged near the grain boundaries, indicating the polarization charges are well compensated, i.e., there should be two-dimensional charge gas confined at grain boundaries. Adjusting the tilt angle of the grain boundaries enables tuning the angle of polarization configurations from 71° to 109°, which in turn allows the control of charge density at the grain boundaries. This general and feasible method opens new doors for the application of charged interfaces in next generation nanoelectronics.

1. Introduction

Interfaces with high density of charges possess some intriguing properties such as insulator–metal transitions [1–3], superconductivity [4,5], magnetoelectric coupling [6–8] and photoconductivity [9,10], which enable charged interfaces to act as active elements in future nanoelectronics [11–13]. These charged interfaces usually occur as either heterointerfaces between different semicondutors and metal oxides [5,14–16] or homointerfaces in ferroic materials such as ferroelectric domain walls [1,17–22]. While heterointerfaces are fixed in space, homointerfaces like charged domain walls in ferroelectrics can serve as powerful tools to control the charged interface due to the switchability of the spontaneous ferroelectric polarization. This phenomenon, which has attracted attention of researchers recently [1,17,20,21], is attributed to the polarization orientation-dependent screening charges at the interface that compensates the depolarization field [23–25]. The formation of a sheet of degenerate charged gas at the interface can exert dramatic changes in local electronic structure and evoke unusual physical properties over a range of several nanometers [26,27].

Unfortunately, charged domain walls with head-to-head or tail-to-tail polarization configurations are typically unstable due to incomplete screening of the bound charges that induce enormous depolarizing fields [26,27]. Nevertheless, there are sparse reports of charged domain walls, which suggest charged interfaces might be energetically favorable under some specific conditions [20,26]. For example, head-to-head and tail-to-tail charged domain walls have been observed in flux-closure domain pattern in $BiFeO_3$/$GdScO_3$ heterostructures [28]. A tetragonal-like crystal structure at the head-to-head charged domain wall can be locally stabilized at the surface and interface of $BiFeO_3$ thin films [24]. In addition,

---

* Corresponding authors.
E-mail addresses: yupu@mail.tsinghua.edu.cn (P. Yu), p-gao@pku.edu.cn (P. Gao).
[1] These authors contributed equally to this work.

https://doi.org/10.1016/j.scib.2020.12.032
2095-9273/

charged domain walls are commonly observed during the ferroelectric switching process [29], although the very tiny size and intermediate nature make them impossible to be manipulated for practical purposes.

Here, we explore the controllability of stable charged interfaces in multiferroic $BiFeO_3$ thin films by grain boundary engineering. $SrTiO_3$ bicrystal substrates are used as templates to grow $BiFeO_3$ thin films with grain boundaries. Results of aberration-corrected scanning transmission electron microscopy (STEM) and piezoresponse force microscopy (PFM) suggest that 10°, 22.6° and 36.8° $BiFeO_3$ grain boundaries exhibit head-to-head polarization configurations. We characterize the atomic structure of these charged grain boundaries and find their width to be as narrow as ~1 nm. The polarization vectors on both sides of grain boundaries suggest unsuppressed polarization near the charged interfaces, indicating the polarization charges are likely to be well screened by mobile charges at grain boundaries. These results validate our strategy and provide a feasible way to obtain tunable charged interfaces in multiferroics via defects engineering for applications in nanoelectronics.

2. Experimental

2.1. Film growth

$BiFeO_3$ thin films were grown via pulsed laser deposition on 10°, 22.6°, and 36.8° $SrTiO_3$ bicrystals. $SrTiO_3$ bicrystals with [001] symmetric tilt grain boundaries were purchased commercially (Shinkosha Co. Ltd.). The orientation relationship of two single crystals is shown in Fig. S1 (online). The tilt angle can be defined as the angle between [100] direction of neighboring $SrTiO_3$ single crystals with [001] as the rotation axis. The temperature and gaseous environment during growth were fixed at 650 °C and 100 mTorr (1 Torr = 133.3 Pa) O_2 respectively. The laser (KrF, λ = 248 nm) energy density was 1.5 J cm^{-2} at the target surface and the repetition rate was 10 Hz for $BiFeO_3$. After the growth, the samples were cooled down to room temperature at 10 °C min^{-1} in 760 Torr oxygen ambient. The sample thickness was controlled by the growth time.

2.2. Samples preparation and STEM characterization

TEM samples were prepared by conventional mechanical polishing and subsequent argon ion milling in a Precision Ion Polishing System 691 (Gatan). The procedure for ion milling consisted of two steps. During the first stage, the guns were operated at 4 keV and at angles of 6°. During the second stage, the guns were operated at 1 keV for 5 min and at angles of 3°, and lowered further to 0.1 keV for 2 min for final surface cleaning. High-angle annular dark-field (HAADF) images and energy-dispersive X-ray spectroscopy (EDS) images in this work were obtained using probe Cs-corrected FEI Titan 60–300 (Titan Themis G2 in Electron Microscopy Laboratory of Peking University) operated at 300 kV. Atom positions were determined by simultaneously fitting two-dimensional Gaussian peaks to a perovskite unit cell using a home-developed code running in MATLAB. Polar displacements of the Fe cations were measured relative to the center of the surrounding Bi cations in HAADF images.

2.3. PFM test

PFM was performed on a commercial scanning probe microscope system (Asylum Research 3D) using commercial Pt/Ir-coated Si tips (Nanosensors) and Pt-coated Si tips (MikroMasch) at room temperature under ambient conditions. The PFM signal was collected at the contact resonance frequency with an AC tip bias of 2 V.

2.4. X-ray diffraction (XRD) test

XRD measurements were carried out with a high-resolution diffractometer (Smartlab, Rigaku) using monochromatic Cu $K_{\alpha1}$ radiation (λ = 1.5406 Å).

3. Results and discussion

50-nm-thick $BiFeO_3$ thin films were deposited on $SrTiO_3$ bicrystal substrates. At room temperature, $BiFeO_3$ with the rhombohedral $R3c$ structure is characterized by two perovskite unit cells connected along their body diagonal [30,31]. All Miller indices of $BiFeO_3$ in this study are based on the pseudocubic lattice. The spontaneous polarization is along the $[111]_{pc}$ axis (where pc denotes pseudocubic indices) [32–34]. The tilt angle β of grain boundaries is tunable as illustrated by the schematic in Fig. 1a. Technically, $BiFeO_3$ could have eight possible polarization orientations in each grain. Due to the epitaxial relationship between films and substrates, grain boundaries in $BiFeO_3$ are expected to vary depending on grain boundaries of the underlying $SrTiO_3$. Fig. 1b depicts three XRD patterns corresponding to the epitaxial $BiFeO_3$ thin films on 10°, 22.6° and 36.8° $SrTiO_3$ bicrystals respectively, all of which clearly exhibit peaks corresponding to $SrTiO_3$ (001) and $BiFeO_3$ (001). The XRD scan in Fig. 1b indicates a high-quality epitaxial single-crystalline nature of $BiFeO_3$ thin films.

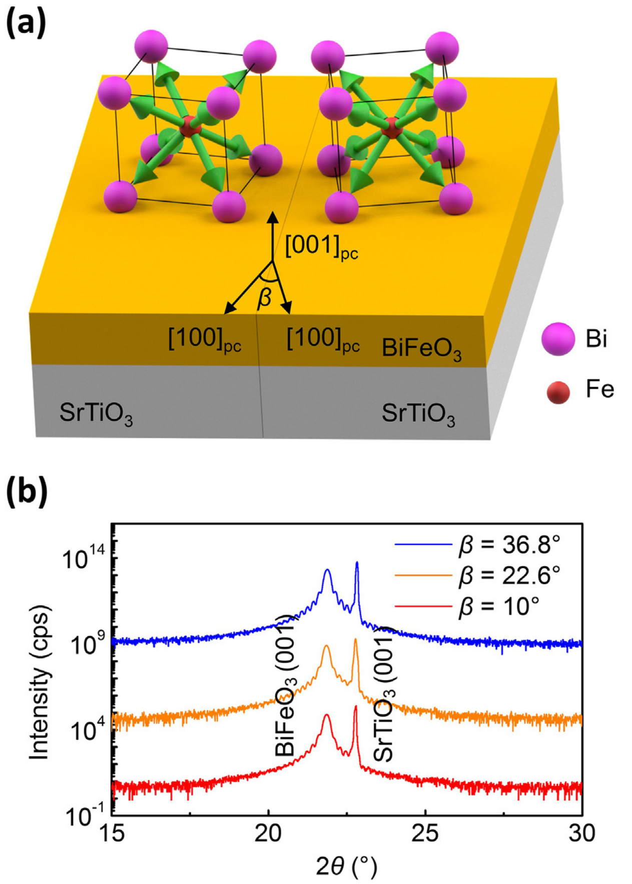

Fig. 1. (Color online) $BiFeO_3$ bicrystal thin film. (a) Schematic diagram of epitaxial $BiFeO_3$ thin films grown on $SrTiO_3$ bicrystal substrates. $BiFeO_3$ have eight possible polarization orientations. (b) XRD profiles of $BiFeO_3/SrTiO_3$ heterostructures revealing the highly crystalline quality of $BiFeO_3$ thin films.

To determine their domain structure, 10°, 22.6° and 36.8° $BiFeO_3$ grain boundaries were subjected to PFM analysis. Topographic and out-of-plane PFM measurements of grain boundaries revealed a small roughness (less than 6 nm) and uniform out-of-plane polarization (Fig. S2 online). Fig. 2a–c show the in-plane measurements near grain boundaries while Fig. 2d–f depict similar measurements in the same areas, albeit in the perpendicular scan directions. We also characterized the polarization orientation at $BiFeO_3/SrTiO_3$ interfaces (Fig. S3 online). The polarization orientation can be clearly determined by the contrast which suggests the head-to-head polarization configuration at grain boundaries. Two uniform constrast regions appear in the vicinity of ~400 nm from each grain boundary, evidencing while near the grain boundaries a monodomain structure exists. Sharp changes in contrast at the grain boundaries resemble those of the domain wall in adjacent $BiFeO_3$ thin films, but the limited resolution of PFM precludes evaluation of their width. The schematics in Fig. 2g–i unambiguously illustrate the polarization configuration at grain boundaries which retain their head-to-head polarization configuration regardless of the grain boundary angle. Moreover, increasing the films to 100 nm in thickness did not evoke a change to the head-to-head polarization configuration of the 10°, 22.6° and 36.8° grain boundaries (Fig. S4 online). In other words, the head-to-head polarization configuration is energetically favorable at these $BiFeO_3$ grain boundaries, which is likely because the positive bound charges can be more effectively screened by negative free carriers in $BiFeO_3$ [35,36]. Bismuth-based ferroelectric oxide films such as $BiFeO_3$ prepared by pulsed laser deposition (PLD) have been reported as n-type semiconductors [36–38], suggesting the negative charges (electrons and negatively charged point defects) in $BiFeO_3$ films could be accumulated at defects such as grain boundaries to screen the positive polarization bound charges. Besides, grain boundaries in oxides usually prefer to be non-stoichiometric which can lead to charge accumulation at these defects [39]. For example, Ti enrichment and deficiency has been reported at different $SrTiO_3$ grain boundaries [40,41], and oxygen vacancy was also detected at yttria-stabilized zirconia grain boundaries [42]. In our cases, the quantitatively elemental analysis of $BiFeO_3$ grain boundaries by EDS indicates the slight deficiency of Bi^{3+} and Fe^{3+} at grain boundaries (Fig. S5 online). Thus, the relative enrichment of oxygen can provide negative charges to screen the positive polarization bound charges at grain boundaries, which stabilizes the head-to-head polarization configurations.

To investigate the structure of charged grain boundaries at atomic scale, 10°, 22.6° and 36.8° grain boundaries were characterized by aberration-corrected STEM. The HAADF image in Fig. 3a shows the atomic structure of the 10° grain boundary. From this *Z*-contrast image [43], it is possible to distinguish the columns comprised of Bi atoms and Fe atoms, respectively. The corresponding fast Fourier transform (FFT) image confirms a tilt angle of 10° in $BiFeO_3$ grain boundary (Fig. S6 online). The width of the 10° grain boundary is about 2 unit cells (~1 nm). The atomic structures of the

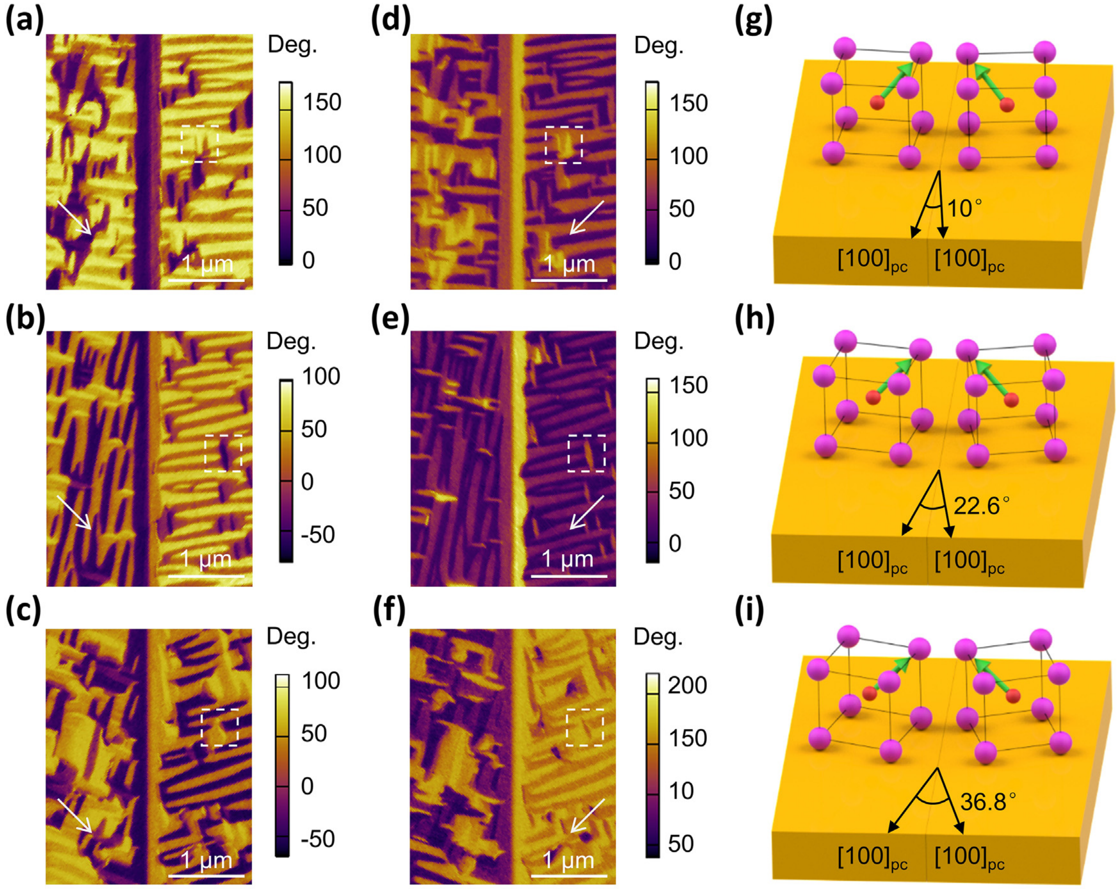

Fig. 2. (Color online) Domain structure of $BiFeO_3$ grain boundaries. (a–c) In-plane PFM measurements for 10°, 22.6° and 36.8° $BiFeO_3$ bicrystals thin films. Arrows indicate scan directions. (d–f) PFM measurements for the same areas of the 10°, 22.6° and 36.8° $BiFeO_3$ bicrystals respectively, albeit in the scan directions perpendicular to those in (a–c). Dashed rectangles denote the same area. Arrows indicate scan directions. (g–i) Schematic diagrams showing polarization configurations near grain boundaries. The green arrows show polarization of $BiFeO_3$ towards the grain boundary.

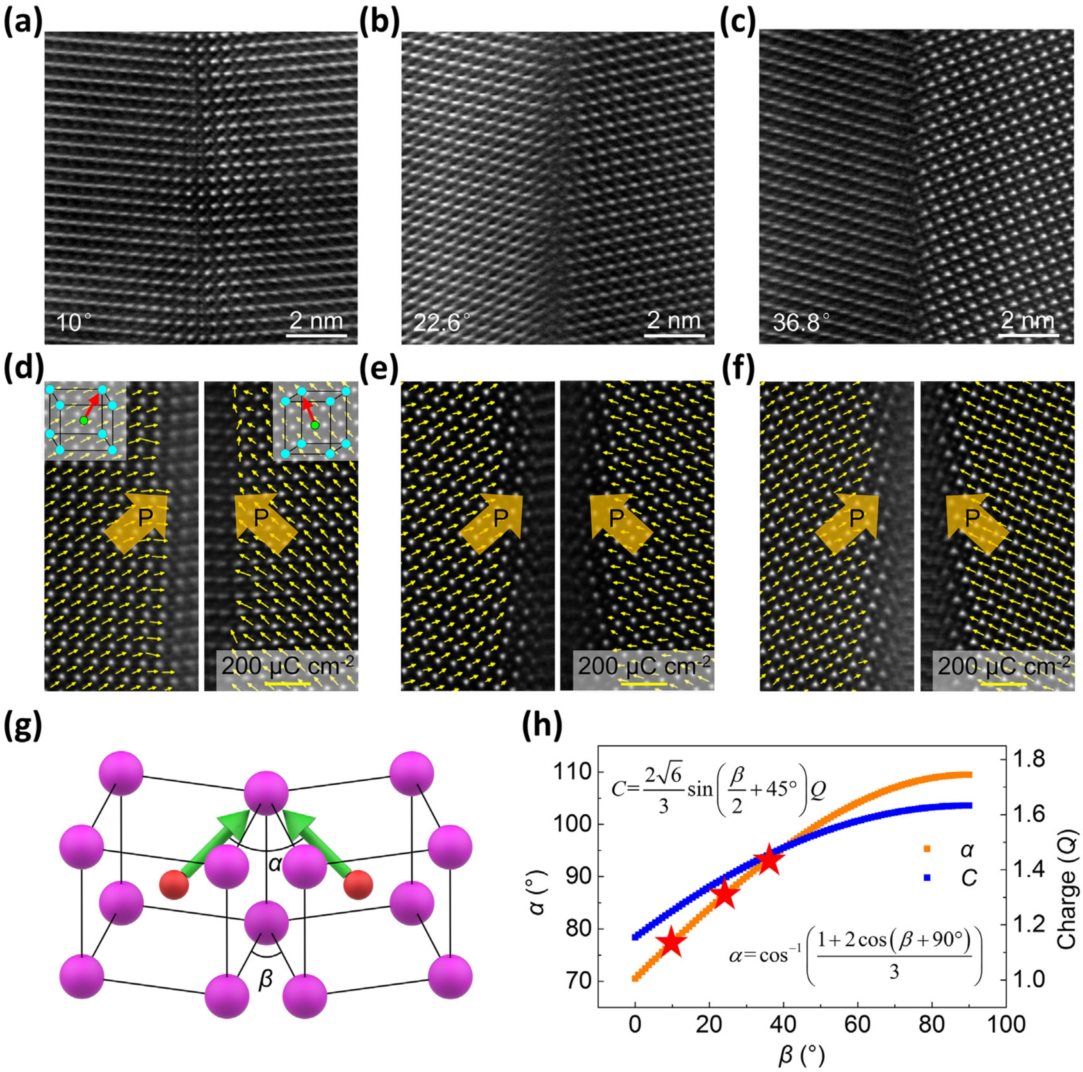

Fig. 3. (Color online) Atomic structure of $BiFeO_3$ grain boundaries. Atomic-resolution HAADF images of (a) 10°, (b) 22.6° and (c) 36.8° $BiFeO_3$ grain boundaries. Atomic images overlaid with polarization vectors of (d) 10°, (e) 22.6° and (f) 36.8° $BiFeO_3$ grain boundaries. The length of arrows indicates the magnitude of the polarization with respect to the yellow scale bar. (g) Schematic diagram of the geometric relationship between grain boundary angle and polarization configuration, where β denotes relative crystal disorientation angle and α denotes angle of polarization orientations. (h) α and charges C at grain boundaries as a function of β. The three stars correspond to 10°, 22.6°, and 36.8° $BiFeO_3$ grain boundaries in this study. Q indicates the polarization of $BiFeO_3$ films.

22.6° and 36.8° grain boundaries are shown in Fig. 3b and c, respectively. Despite many efforts, obtaining perfect atomic structure on both sides of a $BiFeO_3$ grain boundary simultaneously has remained challenging. Zone axes of two grains of $BiFeO_3$ are not consistent, making it difficult to perfectly observe the atomic structure of both grains at the same time. This may be rooted in the distorted structure of the combined rhombohedral $BiFeO_3$ bicrystals without the constraint from the $SrTiO_3$ substrate in plan-view TEM samples [44].

To further elucidate how polarization occurs at the grain boundaries, atomic-resolution images for both sides of grain boundaries were obtained and analyzed separately. From these HAADF images, we can precisely determine the positions of Bi atom columns and Fe atom columns. The polarization vectors of unit cells near the grain boundaries were mapped according to the relative displacement between Fe atom columns and the center of four neighboring Bi atom columns [24]. Fig. 3d depicts the representative HAADF images of the 10° grain boundary overlaid with the corresponding spatial distribution of polarization vectors, where arrow angle and length indicate the orientation and magnification, respectively, of the projected polarization in each unit cell. Conventional understanding suggests that the polarization should be greatly suppressed at the charged interface [22,25]. Nevertheless, the polarization vectors are uniform even near the grain boundary. Similar results were obtained for 22.6° and 36.8° grain boundaries shown in Fig. 3e and f. Fig. 3g shows a schematic representation of α and β (where α is the angle of polarization orientations at $BiFeO_3$ grain boundaries and β is the angle of grain boundaries). The geometric relationship between α and β is shown in Fig. S7 (online, arrows indicate directions of polarization). For simplicity, we consider $BiFeO_3$ a cubic structure. The geometric relationship between α and β can be expressed as

$$\alpha = \cos^{-1}\left(\frac{1+2\cos(\beta+90^\circ)}{3}\right). \tag{1}$$

The 10°, 22.6° and 36.8° grain boundaries exhibit 77°, 86° and 94° head-to-head polarization configurations respectively, indicating that continuous tuning of the angle of charged interfaces can be achieved by adjusting the grain boundary angle of the $SrTiO_3$ bicrystal substrates. Fig. 3h plots this relationship. Therefore, the polarization charge *C* at grain boundaries resulting from head-to-head polarization configurations can be expressed as a function of β which is shown in Fig. 3h. The discrete three points in plots represent the experimental measurements of 10°, 22.6° and 36.8° grain boundaries in this study. These plots can guide strategic design of grain boundaries with tunable polarization charges by manipulating the angle of $SrTiO_3$ bicrystal from 0° to 90°. This general and feasible method creates new avenues towards the development of innovative charged interfaces which are absent in regular multiferroics.

Identifying the atomic structure is critical for a comprehensive understanding of $BiFeO_3$ grain boundaries. Grain boundaries of some crystals such as $SrTiO_3$ have been characterized thoroughly with respect to their atomic structures and local electronic structures via advanced atomic-resolution imaging and electron energy loss spectroscopy [39,40,45]. In contrast, there exist few reports of the atomic structure of $BiFeO_3$ grain boundaries, especially by TEM methods, perhaps due to limitations of the thin-film growth technology and the low mechanical stability of $BiFeO_3$ [46–49]. After many careful attempts, we obtained the atomic structure reported in this study and demonstrated that the width of $BiFeO_3$ grain boundaries can be as narrow as ~1 nm.

The $BiFeO_3$ grain boundary in this study exhibits head-to-head polarization configuration and offers an alternative tool for fabricating tunable charged interfaces in ferroelectric thin films. The width of such grain boundary is as narrow as the as-grown 180°, 109° or 71° domain walls in $BiFeO_3$ thin films [33]. These kinds of charged interfaces possess anomalous polarization configurations compared with conventional 180°, 109° and 71° domain walls in $BiFeO_3$ thin films. They are also robust and therefore retain these polarization configurations despite changes in film thicknesses and external stimuli. Since the maximum grain boundary angle of tilt $SrTiO_3$ bicrystals is 90° (schematically shown in Fig. S7 online), adjusting the angle of $SrTiO_3$ bicrystal from 0° to 90° enables tunable polarization configurations between 71° and 109°, indicating that precise design of the type of such charged interfaces is possible. Such charged grain boundaries are expected to produce many novel properties such as conductivity [18,50], magnetoelectric properties [8] and photoconductivity [9]. Undoubtedly, further research will lead to the discovery of innovative approaches to apply these promising charged grain boundaries and achieve their practical application.

4. Conclusion

In summary, we have presented a general and viable method to create tunable grain boundaries with head-to-head polarization configurations in $BiFeO_3$ thin films. We also demonstrated the atomic structure for 10°, 22.6°, and 36.8° $BiFeO_3$ charged grain boundaries whose single head-to-head polarization configuration and adjacent monodomain structure indicate that charged grain boundaries are uniform and can therefore be readily designed and controlled. Direct observation of the atomic structure of charged grain boundaries via aberration-corrected STEM revealed the identical polarization on either side of the grain boundaries. In addition, the polarization configuration of the charged interfaces was demonstrated to be tunable from 71° to 109° by adjusting the angle of $SrTiO_3$ bicrystal to control interfacial charge density. Our strategy leverages grain boundary engineering for tunable charged interfaces in $BiFeO_3$, although it may be extended to other types of ferroelectric materials with perovskite structure, such as $PbTiO_3$ and $BaTiO_3$. The ability to controllably fabricate charged interfaces offers new routes towards the development of applications of multiferroic thin films in nanoelectronics.

Conflict of interest

The authors declare that they have no conflict of interest.

Acknowledgments

This work at Peking University was supported by the National Basic Research Program of China (2016YFA0300804), the National Natural Science Foundation of China (51672007 and 11974023), Key Area R&D Program of Guangdong Province (2018B010109009), the Key R&D Program of Guangdong Province (2018B030327001), National Equipment Program of China (ZDYZ2015-1), and the "2011 Program" Peking-Tsinghua-IOP Collaborative Innovation Centre for Quantum Matter. This work at Tsinghua University was supported by the National Basic Research Program of China (2016YFA0301004), the National Natural Science Foundation of China (51872155, 52025024), and the Beijing Advanced Innovation Center for Future Chip (ICFC).

Author contributions

Mingqiang Li carried out TEM experiments, analyzed the data and wrote the manuscript under the direction of Peng Gao. Ruochen Shi, Ruixue Zhu, Xiaomei Li and Yang Cheng assisted the data analysis. Shuzhen Yang grew the samples and carried out PFM tests, and Linglong Li carried out conductive atomic force microscopy tests under the direction of Pu Yu. Peng Gao directed the project. The manuscript was written through contributions of all authors. All authors have given approval to the final version of the manuscript.

Appendix A. Supplementary materials

Supplementary materials to this article can be found online at https://doi.org/10.1016/j.scib.2020.12.032.

References

[1] Seidel J. Topological structures in ferroic materials. Switzerland: Springer International Publishing 2016.
[2] Thiel S, Hammerl G, Schmehl A, et al. Tunable quasi-two-dimensional electron gases in oxide heterostructures. Science 2006;313:1942–5.
[3] Tian G, Yang W, Song X, et al. Manipulation of conductive domain walls in confined ferroelectric nanoislands. Adv Funct Mater 2019;29:1807276.
[4] Gozar A, Logvenov G, Kourkoutis LF, et al. High-temperature interface superconductivity between metallic and insulating copper oxides. Nature 2008;455:782–5.
[5] Herranz G, Basletić M, Bibes M, et al. High mobility in $LaAlO_3/SrTiO_3$ heterostructures: origin, dimensionality, and perspectives. Phys Rev Lett 2007;98:216803.
[6] Chakhalian J, Freeland JW, Srajer G, et al. Magnetism at the interface between ferromagnetic and superconducting oxides. Nat Phys 2006;2:244–8.
[7] Gupta R, Chaudhary S, Kotnala RK. Interfacial charge induced magnetoelectric coupling at $BiFeO_3/BaTiO_3$ bilayer interface. ACS Appl Mater Interfaces 2015;7:8472–9.
[8] Kumari S, Ortega N, Kumar A, et al. Dielectric anomalies due to grain boundary conduction in chemically substituted $BiFeO_3$. J Appl Phys 2015;117:114102.
[9] Nandy S, Mocherla PSV, Sudakar C. Photoconductivity induced by nanoparticle segregated grain-boundary in spark plasma sintered $BiFeO_3$. J Appl Phys 2017;121:203102.
[10] Liu S, Zheng F, Koocher NZ, et al. Ferroelectric domain wall induced band gap reduction and charge separation in organometal halide perovskites. J Phys Chem Lett 2015;6:693–9.
[11] Hwang HY, Iwasa Y, Kawasaki M, et al. Emergent phenomena at oxide interfaces. Nat Mater 2012;11:103–13.
[12] Catalan G, Seidel J, Ramesh R, et al. Domain wall nanoelectronics. Rev Mod Phys 2012;84:119–56.
[13] Seidel J. Domain walls as nanoscale functional elements. J Phys Chem Lett 2012;3:2905–9.
[14] Niranjan MK, Wang Y, Jaswal SS, et al. Prediction of a switchable two-dimensional electron gas at ferroelectric oxide interfaces. Phys Rev Lett 2009;103:016804.
[15] Liu Y, Zhu Y-L, Tang Y-L, et al. Local enhancement of polarization at $PbTiO_3/BiFeO_3$ interfaces mediated by charge transfer. Nano Lett 2017;17:3619–28.

[16] Ohtomo A, Hwang HY. A high-mobility electron gas at the $LaAlO_3/SrTiO_3$ heterointerface. Nature 2004;427:423–6.
[17] Fujisawa H, Seto S, Nakashima S, et al. Introduction of an artificial domain wall into $BiFeO_3$ thin film using $SrTiO_3$ bicrystal substrate. Jpn J Appl Phys 2015;54:10NA06.
[18] Rodriguez BJ, Chu YH, Ramesh R, et al. Ferroelectric domain wall pinning at a bicrystal grain boundary in bismuth ferrite. Appl Phys Lett 2008;93:142901.
[19] Marincel DM, Zhang H, Kumar A, et al. Influence of a single grain boundary on domain wall motion in ferroelectrics. Adv Funct Mater 2014;24:1409–17.
[20] Gureev MY, Tagantsev AK, Setter N. Head-to-head and tail-to-tail 180° domain walls in an isolated ferroelectric. Phys Rev B 2011;83:184104.
[21] Feigl L, Sluka T, McGilly LJ, et al. Controlled creation and displacement of charged domain walls in ferroelectric thin films. Sci Rep 2016;6:31323.
[22] Tang YL, Zhu YL, Wang YJ, et al. Atomic-scale mapping of dipole frustration at 90 degrees charged domain walls in ferroelectric $PbTiO_3$ films. Sci Rep 2014;4:4115.
[23] Li M, Cheng X, Li N, et al. Atomic-scale mechanism of internal structural relaxation screening at polar interfaces. Phys Rev B 2018;97:180103.
[24] Li L, Gao P, Nelson CT, et al. Atomic scale structure changes induced by charged domain walls in ferroelectric materials. Nano Lett 2013;13:5218–23.
[25] Jia C-L, Mi S-B, Urban K, et al. Atomic-scale study of electric dipoles near charged and uncharged domain walls in ferroelectric films. Nat Mater 2008;7:57–61.
[26] Eliseev EA, Morozovska AN, Svechnikov G, et al. Static conductivity of charged domain walls in uniaxial ferroelectric semiconductors. Phys Rev B 2011;83:235313.
[27] Sturman B, Podivilov E, Stepanov M, et al. Quantum properties of charged ferroelectric domain walls. Phys Rev B 2015;92:214112.
[28] Qi Y, Chen Z, Huang C, et al. Coexistence of ferroelectric vortex domains and charged domain walls in epitaxial $BiFeO_3$ film on $(110)_O$ $GdScO_3$ substrate. J Appl Phys 2012;111:104117.
[29] Han M-G, Marshall MSJ, Wu L, et al. Interface-induced nonswitchable domains in ferroelectric thin films. Nat Commun 2014;5:4693.
[30] Ederer C, Spaldin NA. Effect of epitaxial strain on the spontaneous polarization of thin film ferroelectrics. Phys Rev Lett 2005;95:257601.
[31] Zavaliche F, Yang SY, Zhao T, et al. Multiferroic $BiFeO_3$ films: domain structure and polarization dynamics. Phase Transit 2006;79:991–1017.
[32] Cruz MP, Chu YH, Zhang JX, et al. Strain control of domain-wall stability in epitaxial $BiFeO_3$ (110) films. Phys Rev Lett 2007;99:217601.
[33] Wang Y, Nelson C, Melville A, et al. $BiFeO_3$ domain wall energies and structures: a combined experimental and density functional theory + U study. Phys Rev Lett 2013;110:267601.
[34] Rossell MD, Erni R, Prange MP, et al. Atomic structure of highly strained $BiFeO_3$ thin films. Phys Rev Lett 2012;108:047601.
[35] Seidel J, Martin LW, He Q, et al. Conduction at domain walls in oxide multiferroics. Nat Mater 2009;8:229–34.
[36] Liu Z, Yan F, Hintzen H. The application of bismuth-based oxides in organic-inorganic hybrid photovoltaic devices. J Am Ceram Soc 2012;95:1944–8.
[37] You T, Shuai Y, Luo W, et al. Exploiting memristive $BiFeO_3$ bilayer structures for compact sequential logics. Adv Funct Mater 2014;24:3357–65.
[38] Farokhipoor S, Noheda B. Conduction through 71 degrees domain walls in $BiFeO_3$ thin films. Phys Rev Lett 2011;107:127601.
[39] Gao P, Yang S, Ishikawa R, et al. Atomic-scale measurement of flexoelectric polarization at $SrTiO_3$ dislocations. Phys Rev Lett 2018;120:267601.
[40] Takehara K, Sato Y, Tohei T, et al. Titanium enrichment and strontium depletion near edge dislocation in strontium titanate [001]/(110) low-angle tilt grain boundary. J Mater Sci 2014;49:3962–9.
[41] Li X, Chen S, Li M, et al. Atomic origin of Ti-deficient dislocation in $SrTiO_3$ bicrystals and their electronic structures. J Appl Phys 2019;126:174106.
[42] Feng B, Lugg NR, Kumamoto A, et al. Direct observation of oxygen vacancy distribution across yttria-stabilized zirconia grain boundaries. ACS Nano 2017;11:11376–82.
[43] Pennycook SJ, Boatner LA. Chemically sensitive structure-imaging with a scanning transmission electron microscope. Nature 1988;336:565–7.
[44] Chen ZH, Damodaran AR, Xu R, et al. Effect of "symmetry mismatch" on the domain structure of rhombohedral $BiFeO_3$ thin films. Appl Phys Lett 2014;104:182908.
[45] Buban JP, Chi M, Masiel DJ, et al. Structural variability of edge dislocations in a $SrTiO_3$ low-angle [001] tilt grain boundary. J Mater Res 2009;24:2191–9.
[46] Rodriguez BJ, Choudhury S, Chu Y, et al. Unraveling deterministic mesoscopic polarization switching mechanisms: spatially resolved studies of a tilt grain boundary in bismuth ferrite. Adv Funct Mater 2009;19:2053–63.
[47] Zeches RJ, Rossell M, Zhang J, et al. A strain-driven morphotropic phase boundary in $BiFeO_3$. Science 2009;326:977–80.
[48] Zhang J, Ke X, Gou G, et al. A nanoscale shape memory oxide. Nat Commun 2013;4:3768.
[49] Yu P, Luo W, Yi D, et al. Interface control of bulk ferroelectric polarization. Proc Natl Acad Sci USA 2012;109:9710–5.
[50] Lin Ye, Fang S, Su D, et al. Enhancing grain boundary ionic conductivity in mixed ionic–electronic conductors. Nat Commun 2015;6:7824.

Mingqiang Li is currently a Ph.D. candidate in Department of Materials Science and Engineering, University of Toronto. He received his M.Sc. degree in Condensed Matter Physics from Peking University in 2020, and B.E. degree from Zhengzhou University in 2016. His research interest focuses on the structure-property relationships of ferroelectrics and nanomaterials by using *in situ* transmission electron microscopy.

Shuzhen Yang received his Ph.D. degree from Department of Physics, Tsinghua University in 2019. He mainly studied the interfacial properties of multiferroic materials, such as $BiFeO_3$, and used piezoelectric force microscopes to study the properties of ferroelectric domain walls and domains.

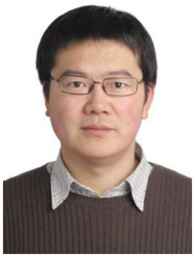

Pu Yu is a professor at Department of Physics, Tsinghua University. He received his Ph.D. degree in Physics from University of California at Berkeley in 2011. After one-year postdoc stay at RIKEN, he joined the faculty of Tsinghua University as an assistant professor in 2012, and was promoted to associate professor in 2017 and then professor in 2018. His current research interest lies in understanding and designing novel electronic states within complex oxide heterostructures.

Peng Gao is an assistant professor in School of Physics, Peking University. He received his Ph.D. degree in Condensed Mater Physics from the Institute of Physics, Chinese Academy of Sciences in 2010. He was a postdoctor in University of Michigan (2010–2013), research associate in Brookhaven National Lab (2013–2014), research fellow and Japan Society for the Promotion of Science (JSPS) foreign fellow in University of Tokyo (2014–2015). He joined Peking University in 2015. His main research interest is probing interfaces in quantum materials via electron scattering.